



**Michigan
Technological
University**

Michigan Technological University
Digital Commons @ Michigan Tech

Michigan Tech Publications

3-2023

Austenite Formation and Manganese Partitioning during Double Soaking of an Ultralow Carbon Medium-Manganese Steel

Josh J. Mueller

Michigan Technological University, muellerj@mtu.edu

Alexandra G. Glover

Michigan Technological University, agglover@mtu.edu

David K. Matlock

Colorado School of Mines

John G. Speer

Colorado School of Mines

Emmanuel De Moor

Colorado School of Mines

Follow this and additional works at: <https://digitalcommons.mtu.edu/michigantech-p>



Part of the [Materials Science and Engineering Commons](#)

Recommended Citation

Mueller, J., Glover, A. G., Matlock, D., Speer, J., & De Moor, E. (2023). Austenite Formation and Manganese Partitioning during Double Soaking of an Ultralow Carbon Medium-Manganese Steel. *Steel Research International*. <http://doi.org/10.1002/srin.202200947>

Retrieved from: <https://digitalcommons.mtu.edu/michigantech-p/17032>

Follow this and additional works at: <https://digitalcommons.mtu.edu/michigantech-p>



Part of the [Materials Science and Engineering Commons](#)

Austenite Formation and Manganese Partitioning during Double Soaking of an Ultralow Carbon Medium-Manganese Steel

Josh J. Mueller,* Alexandra G. Glover, David K. Matlock, John G. Speer, and Emmanuel De Moor

Double soaking (DS) is a thermal processing route intended to produce austenite–martensite microstructures in steels containing austenite-stabilizing additions and consists of intercritical annealing (primary soaking), followed by heating and brief isothermal holding at an increased temperature (secondary soaking), and quenching. Herein, experimental dilatometry during DS of a medium-manganese (Mn) steel with nominally 7 wt% Mn and an ultralow residual carbon concentration, in combination with phase-field simulations of austenite formation during secondary soaking, is presented. The feasibility of maintaining heterogeneous Mn distributions during DS is demonstrated and insight is provided on the effects of the secondary soaking temperature and prior Mn distribution on the ferrite-to-austenite phase transformation during the secondary soaking portion of the DS treatment.

termed double soaking (DS), has been developed which may be used to generate martensite–austenite microstructures. Application of the DS heat treatment to a 0.14C–7.14Mn steel has been shown to produce an attractive combination of mechanical properties including: yield strength and ultimate tensile strength of 950 and 1700 MPa, respectively, while maintaining 12.5% ductility and eliminating yield point elongation.^[12–14] The DS treatment consists of a primary soak step at an intercritical temperature, similar to IA, followed by a secondary soak step at a greater temperature and cooling down to room temperature. During the primary soak, some fraction of ferrite (and carbides if present) may transform to as primary austenite. The remaining Mn-deficient ferrite transforms to austenite during the secondary soak at a higher temperature, referred to as secondary austenite. Secondary soak times are relatively short and intended to avoid extensive redistribution of austenite-stabilizing solute among the primary and secondary austenite. Without the requisite solute enrichment to stabilize secondary austenite to room temperature, the secondary austenite will transform to martensite upon cooling. The solute-enriched primary austenite may be retained upon cooling if it has sufficient solute enrichment.

The thermodynamic conditions influencing the ferrite-to-austenite phase transformation during the primary soak are conducive to a partitioning transformation, where austenite forms with Mn enrichment as Mn is diffusively transported through ferrite to the austenite–ferrite interface. Despite the rapid diffusivity of solute C, the growth of intercritical austenite has been suggested to be predominantly controlled by Mn diffusion in circumstances where Mn-enriched cementite is slow to dissolve.^[15] The thermodynamic conditions influencing austenite growth during the secondary soak are different than during the primary soak. After primary soaking, Mn is expected to be heterogeneously distributed between ferrite and austenite. Mn redistribution during secondary soaking is expected to depend on the phase-transformation mechanism associated with the growth of secondary austenite. If secondary austenite growth proceeds by means of a partitioning transformation, additional Mn redistribution would be expected. However, if the transformation is of the massive type, the Mn distribution is expected to remain nearly

tenite, referred to as primary austenite. The remaining Mn-deficient ferrite transforms to austenite during the secondary soak at a higher temperature, referred to as secondary austenite. Secondary soak times are relatively short and intended to avoid extensive redistribution of austenite-stabilizing solute among the primary and secondary austenite. Without the requisite solute enrichment to stabilize secondary austenite to room temperature, the secondary austenite will transform to martensite upon cooling. The solute-enriched primary austenite may be retained upon cooling if it has sufficient solute enrichment.

1. Introduction

Austenite–ferrite microstructures can be generated in medium-manganese (Mn) steels when solute-enriched austenite is formed during intercritical annealing (IA) and stabilized to room temperature.^[1–11] Recently, a novel thermal processing route,

J. J. Mueller, A. G. Glover
J-2: Dynamic Structure Design, Engineering, & Vessel Operations
Los Alamos National Laboratory
Los Alamos, NM 87545, USA
E-mail: jmueller@lanl.gov, muellerj@mtu.edu

J. J. Mueller, A. G. Glover, D. K. Matlock, J. G. Speer, E. De Moor
Advanced Steel Processing and Products Research Center
Colorado School of Mines
1500 Illinois St, Golden, CO 80401, USA

J. J. Mueller, A. G. Glover
Materials Science and Engineering Department
Michigan Technological University
1400 Townsend Dr, Houghton, MI 49931, USA

 The ORCID identification number(s) for the author(s) of this article can be found under <https://doi.org/10.1002/srin.202200947>.

© 2023 The Authors. Steel Research International published by Wiley-VCH GmbH. This is an open access article under the terms of the Creative Commons Attribution-NonCommercial-NoDerivs License, which permits use and distribution in any medium, provided the original work is properly cited, the use is non-commercial and no modifications or adaptations are made.

DOI: 10.1002/srin.202200947

bimodal, initially, as the secondary austenite would inherit the composition of the ferrite.^[16–19]

The medium-Mn steel with nominally 7 wt% Mn (referred to as 7Mn) used in the present study has an ultralow residual C content; a previous investigation of this identical steel indicated that substantial Mn-partitioning-induced austenite growth can occur during 1000 s IA treatments.^[20] The present study discusses microstructural evolution of this 7Mn steel during DS treatments. The composition of the 7Mn steel was not conducive to full stabilization of primary austenite to room temperature, and thus dilatometry during thermal processing was conducted to characterize the relative stability of primary and secondary austenite. Experimental observations and simulation predictions are presented pertaining to Mn redistribution and the phase-transformation mechanisms of secondary austenite formation during secondary soaking. Dilatometry results obtained during cooling support the viability of a heterogeneous Mn distribution being maintained during secondary soaking. Additionally, MICRESS simulations of heating and secondary soaking, along with thermodynamic analysis utilizing Gibbs free energy–Mn concentration curves from Thermo-Calc, provide context on how the secondary soaking temperature (SST) affects the formation of secondary austenite and the redistribution of Mn during the secondary soak.

2. Experimental Section

The composition of the steel studied in this investigation was Fe–0.0005C–7.19Mn–0.25Si (wt%). The as-received material was cast from a vacuum melt, reheated to 1230 °C, and hot-rolled to a thickness of 2.87 mm before being cold-rolled to a thickness of 1.42 mm. Additional studies published on this steel are available elsewhere.^[20,21]

All thermal processing presented here was accomplished in a TA Instruments Dil 805L dilatometer. The DS heat treatments consisted of heating at 50 °C s^{−1} to a primary soaking temperature (PST), isothermal holding for 1000 s, heating at 10 °C s^{−1} to an SST of 850 °C, isothermal holding for 5 s, followed by quenching to room temperature at 20 °C s^{−1}. The rapid heating rate of 50 °C s^{−1} was chosen to minimize any effects during heating to the PST; a more gradual heating rate was chosen for heating from the PST to the SST to minimize potential artifacts caused by rapid heating rates. Different PSTs, ranging from 640 to 710 °C, were investigated. To compare the dilation response during DS against direct austenitization (i.e., without a primary soaking step), additional samples were heated from room temperature to 800 °C at 50 °C s^{−1}, held for 5 s, and quenched to room temperature at 20 °C s^{−1}. Equilibrium calculations from the TCFE9 database of Thermo-Calc indicated an A_{e3} temperature of 698 °C for the 7Mn steel, which suggested that 800 °C was sufficient to fully austenitize samples from the initial condition. The SST of 850 °C was necessary to induce full austenitization in the DS samples due to the Mn partitioning that occurs during the PS; this is discussed in further in Results section.

Simulations of microstructural evolution during secondary soaking were conducted using MICRESS coupled to the TCFE9 and MOBFE4 Thermo–Calc databases. These simulations considered an Fe–7.2Mn composition with an equiaxed

initial microstructure that represented equilibrium austenite and ferrite fractions, and equilibrium Mn concentrations corresponding to a PST of 640 °C. The initial grain size, approximately 1 μm, was chosen to reflect the grain refinement typical of medium-Mn steels after IA. Simulations included heating at 10 °C s^{−1} from 640 °C to an SST and isothermal holding for 1000 s. Relevant simulation parameters are listed in Table 1. The assumed value for interface energy was identical to that used by Zhu and Miltzer, and values relating to interface mobility and diffusivity were based on those reported in literature or sourced from the MOBFE4 Thermo–Calc database.^[22–28]

3. Results

3.1. Dilatometry

The relative dilation with temperature is summarized in Figure 1a for a sample that underwent a DS treatment with a PST of 660 °C. Figure 1b,c shows magnified views of the boxed regions in Figure 1a and indicate some common features characteristic of microstructural evolution during DS. Other samples, discussed later, underwent similar DS treatments with PSTs ranging from 640 to 710 °C and display similar dilation features to those indicated in Figure 1. Linear thermal expansion upon heating to the PST is shown Figure 1a,b which was immediately followed by isothermal contraction of the sample at the PST associated with the transformation of ferrite to primary austenite (γ_p). During subsequent heating to the SST, thermal expansion was observed which was interrupted by another contraction associated with the transformation of the remaining ferrite to secondary austenite (γ_s). With continued heating, the ferrite-to-austenite transformation completes at approximately 760 °C followed by linear thermal expansion until reaching the SST. Upon cooling, the sample exhibited thermal contraction. As shown in Figure 1a,c, the linear contraction during cooling was interrupted at two temperatures; these interruptions, labeled M_I and M_{II}, are interpreted as two distinct martensite-transformation events. M_I occurred first during cooling and is suggested to correspond to the transformation of Mn-lean γ_s to martensite. As the martensite transformation of γ_s progressed toward completion, the associated expansion reduced, and thermal contraction was again the predominant influence in the dilation response. M_{II} is suggested to correspond to the transformation of solute-rich γ_p to martensite and occurred at a lower temperature relative to M_I. Note that the net relative dilation was negative upon returning to room temperature; this suggests incomplete martensite transformation, and that the sample contained some retained austenite following the DS treatment.

Table 1. MICRESS parameters for DS simulations.

Interface Energy [J m ^{−2}]		0.8
Interface mobility	M ₀ [cm ⁴ s ^{−1}]	1
	ΔG* [kJ mol ^{−1}]	140
Mn diffusivity in α	D ₀ [cm ² s ^{−1}]	1.49
	Q [kJ mol ^{−1}]	233.6
Mn diffusivity in γ		MOBFE4

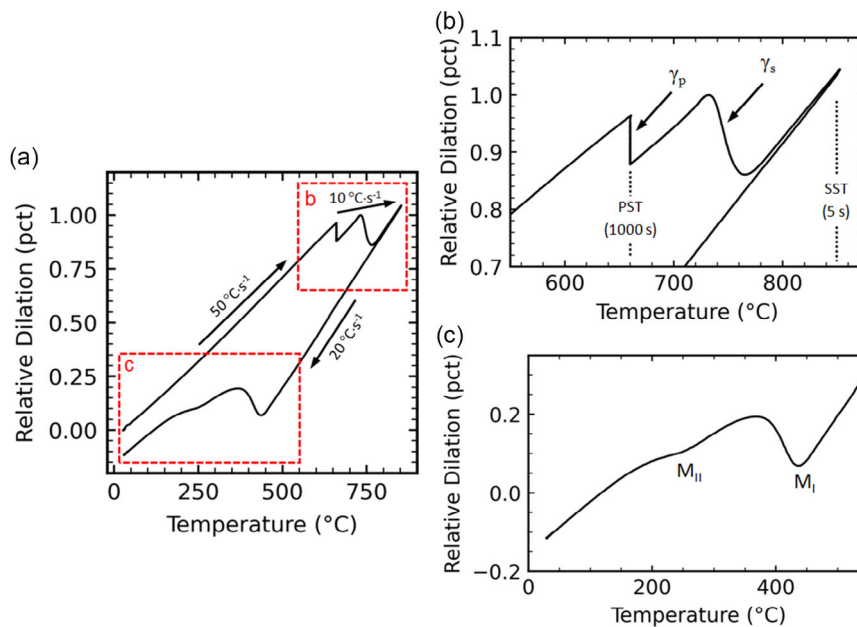


Figure 1. a) Dilatometry results from a sample that underwent a double-soaking (DS) treatment with a primary soaking temperature (PST) of 660 °C. Enlarged views of boxed regions in a) b) labeled “b” and c) labeled “c.”

The relative dilation of samples during DS heat treatments with PSTs ranging from 640 to 710 °C is shown in **Figure 2** along with a sample that was austenitized and quenched directly from the initial, cold-rolled condition. Consistent with the features identified in Figure 1, dilation data corresponding to PSTs ranging from 640 to 700 °C indicate formation of γ_p and γ_s . Although the PST of 700 °C slightly exceeds the calculated A_{e3} temperature from the TCFE9 database of Thermo-Calc (698 °C), Mn-banding in the sample likely caused the Mn-lean bands to have a local A_3 temperature that exceeded the nominal A_{e3} temperature of the alloy. Additional discussion of the banded microstructure in this steel can be found in a previous study.^[20] The absence of appreciable γ_s formation in the 710 °C PST sample suggests that 710 °C was sufficient to overcome the effect from Mn-banding and that transformation of ferrite to austenite completed during the primary soak. The A + Q sample indicates full transformation of ferrite to austenite during heating to 800 °C, exhibiting 50 °C s^{-1} A_{c1} and A_{c3} temperatures of approximately 710 and 760 °C, respectively. Note that while the ferrite-to-austenite transformation in the A + Q sample had reached completion at approximately 760 °C, the transformation in the DS samples did not reach completion until greater temperatures were reached. This is the justification for the greater SST used in the DS samples relative to the austenitizing temperature used for the A + Q sample; it is also a consequence of the Mn partitioning that occurred during the primary soak. The Mn concentration in the remaining ferrite after the primary soak decreased with increasing PST and required heating to greater temperatures to transform to austenite. Close inspection of Figure 2 indicates that the secondary austenite formation shifts to greater temperatures with increasing PST. It should also be noted that the 690, 700, and 710 °C, and A + Q samples exhibit a small contraction during heating immediately prior to austenite formation;

this is believed to be an artifact associated with initial austenite formation caused by the high heating rate and thermal gradients within the sample.

The samples with PSTs of 640–700 °C exhibit M_I and M_{II} transformations upon cooling, although, these transformation events overlap considerably in the 690 and 700 °C PST samples. Both the 710 °C PST and A + Q samples exhibit a single expansion upon cooling that is interpreted to reflect martensite transformation of austenite with a relatively homogeneous Mn distribution. Comparison of the dilation responses during cooling of the DS samples to the A + Q sample suggests that the primary soak step can generate a heterogeneous Mn distribution which persists through full austenitization. Additionally, DS samples with PSTs of 680 °C and lower indicated a negative relative dilation upon cooling down to room temperature. This suggests incomplete martensite transformation due to greater corresponding Mn enrichment and stability of the γ_p relative to samples with PSTs of 690 °C and greater.

The M_I and M_{II} temperatures corresponding to each PST were identified by plotting the derivative of the dilation with respect to temperature against the corresponding temperature during cooling. **Figure 3a** shows a representative example of how the M_I and M_{II} temperatures were identified from the derivative of the relative dilation with temperature. The M_I and M_{II} temperatures corresponding to DS treatments with different PSTs are plotted in Figure 3b. With increasing PST, the M_{II} temperature increased, reducing the difference between M_I and M_{II} temperatures.

The transformation temperature data plotted in Figure 3b were used to predict the Mn concentrations in the corresponding γ_p and γ_s using the following equation based on the empirical relation developed by Mahieu et al.^[29] for the effect of solute concentration in austenite on the martensite start temperature

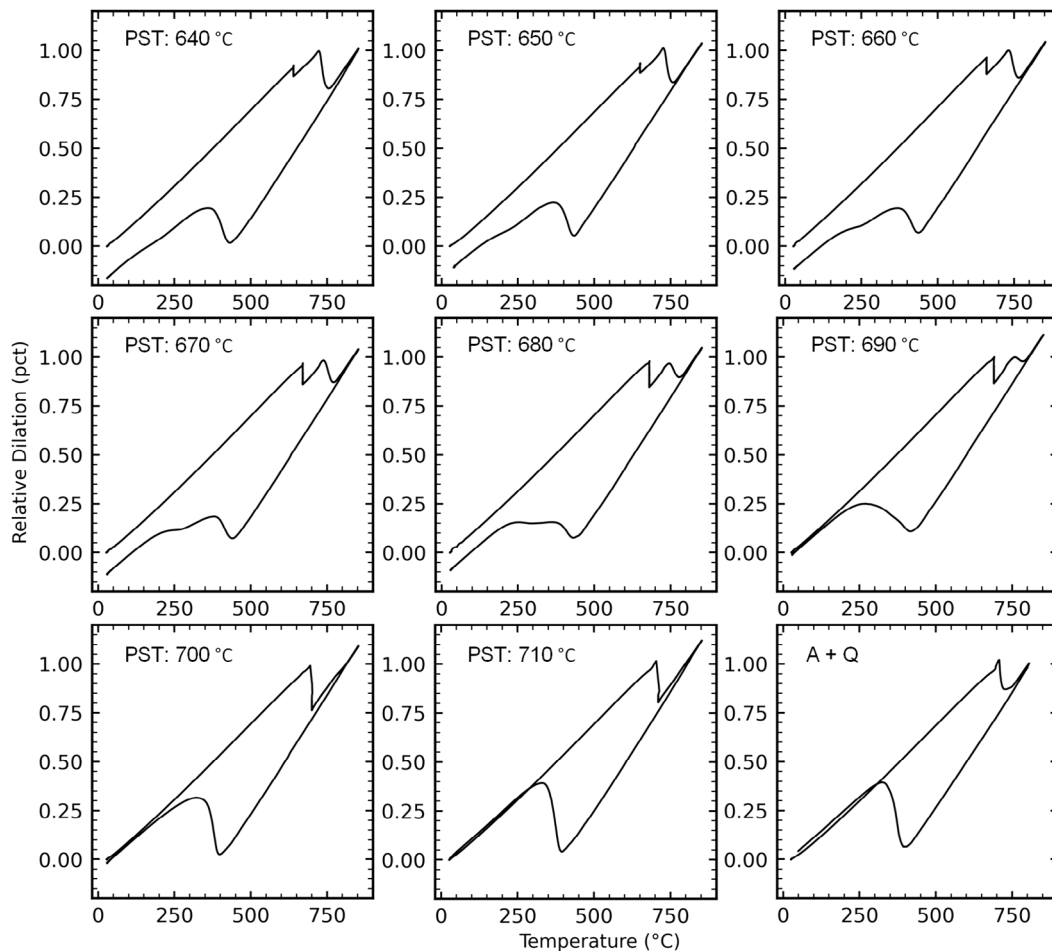


Figure 2. Dilatometry results from samples that underwent a DS treatment with PSTs ranging from 640 to 710 °C; the corresponding PST is labeled in each plot. The bottom right plot labeled “A + Q” corresponds to a sample that was austenitized directly from the initial, as-rolled condition and quenched.

$$M = 539 - 423(C) - 30.4(\text{Mn}) - 7.5(\text{Si}) + 30(\text{Al}) \quad (1)$$

where M corresponds to the transformation temperature (M_I or M_{II}) and Mn, Si, and Al are the manganese, silicon, and aluminum concentrations of the parent austenite in wt% (γ_s or γ_p , respectively). The composition of the steel studied here is essentially an Fe–Mn binary alloy, which enables calculation of the corresponding Mn concentrations without convolution from other alloy elements. The calculated Mn concentrations associated with γ_p and γ_s are plotted in Figure 3c along with the equilibrium values determined using ThermoCalc for the Mn concentrations of intercritical ferrite (α) and austenite (γ) at the corresponding PSTs. A previous study on this steel, which utilized IA times and temperatures identical to the primary soak in the present study, indicated that the Mn enrichment in austenite formed during IA treatments increased with decreasing IA temperature; this trend is consistent with equilibrium assumptions.^[20] The data shown in Figure 3c are also consistent with equilibrium assumptions. The calculated Mn concentrations of the γ_p exhibit a similar trend compared to the equilibrium calculations for intercritical γ , while the calculated Mn concentrations of γ_s are in good

agreement with the equilibrium calculation for intercritical α ; this suggests that the Mn distributions that developed during the primary soak portions of the DS treatments were largely retained through the secondary soak.

3.2. Simulation of Microstructural Evolution

The commercial phase-field software MICRESS was utilized to simulate microstructural evolution during the secondary soak step of the DS treatment. The initial simulation structure is shown in Figure 4a and represents the microstructure upon completion of a primary soak step with a PST of 640 °C. The initial simulation structure corresponds to equilibrium calculations from ThermoCalc with an initial austenite fraction of 0.55, and Mn concentrations in austenite and ferrite of 10.6 and 2.9 wt%, respectively. The simulations included heating at 10 °C s⁻¹ from 640 °C to an SST of either 750 or 850 °C.

The resulting Mn distribution and phase map after heating to 750 °C and secondary soaking for 1000 s are shown in Figure 4b. Note that the phase map does not differentiate γ_p and γ_s . Since these simulations considered microstructural evolution during the secondary soak, formation of additional austenite in the

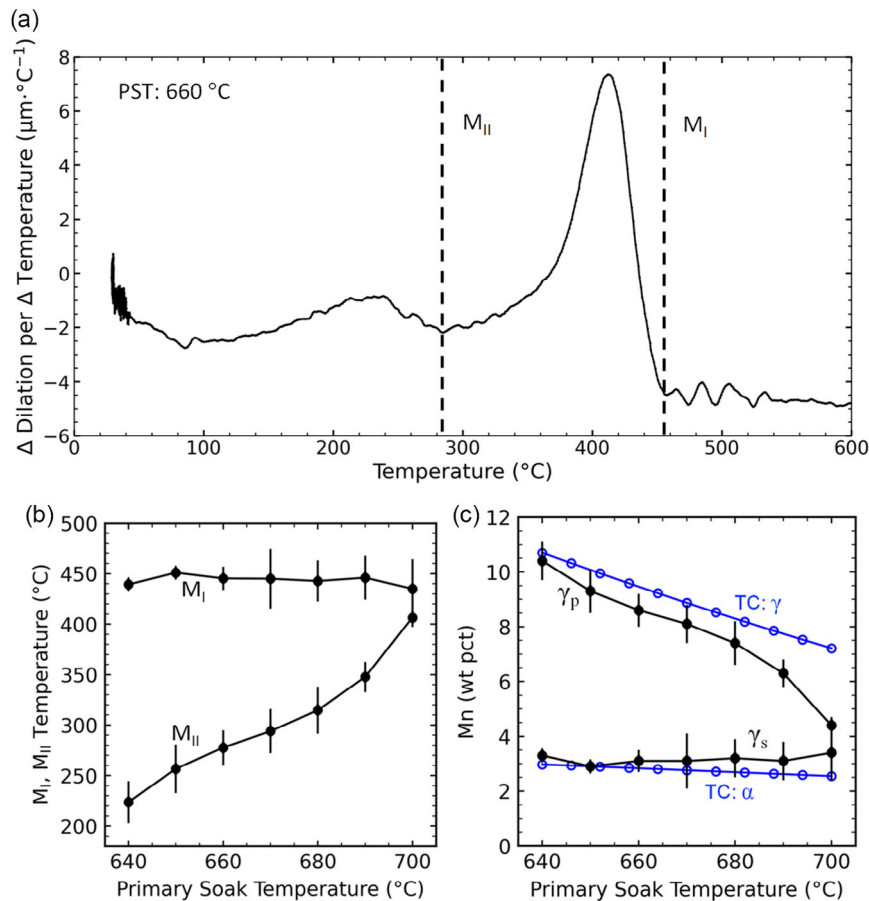


Figure 3. a) Derivative of dilation with respect to temperature during cooling plotted against temperature for a sample that underwent a DS treatment with a PST of 660 $^{\circ}\text{C}$. Dashed, vertical lines indicate approximate temperatures identified as M_I and M_{II} . b) M_I and M_{II} temperatures corresponding to DS treatments using different PSTs shown in Figure 2. c) Calculated Mn concentration in γ_p and γ_s from M_{II} and M_I temperature measurements, respectively (black, filled circles), and equilibrium Thermo-Calc calculations for Mn concentrations in austenite (TC: γ) and ferrite (TC: α) for different PSTs (blue, open circles). Mean and standard deviation are plotted from three measurements at each PST in (b) and (c).

simulations corresponds to γ_s . Comparison of the phase maps and the Mn concentration maps in Figure 4a,b reveals that the γ_s , which corresponds to the red regions in the Mn map of Figure 4b, has an intermediate Mn concentration of approximately 5 wt%. It is interesting to note that the Mn concentration of the remaining α at 1000 s in the 750 $^{\circ}\text{C}$ SST simulation was reduced relative to the initial α concentration, while the Mn concentration in the γ_p was not reduced. These results are consistent with γ_s formation at 750 $^{\circ}\text{C}$ that proceeds by means of a Mn-partitioning-induced transformation.

Results from the simulation that considered an SST of 850 $^{\circ}\text{C}$ are shown in Figure 5. Figure 5a displays the phase map and Mn distribution map that correspond to a temperature of 810 $^{\circ}\text{C}$ during heating to the SST and, compared to the initial condition in Figure 4a, indicate that γ_s has already consumed some of the α before reaching the SST. The Mn concentration map reveals that the γ_s formed does not correspond to an intermediate Mn concentration, such as in Figure 4b for the 750 $^{\circ}\text{C}$ SST simulation. Rather, the γ_s inherited the Mn concentration of the α . This suggests that formation of γ_s proceeded by means of a massive transformation.^[16–19] The simulation results after secondary

soaking at 850 $^{\circ}\text{C}$ for 5 and 1000 s are shown in Figure 5b and c, respectively. At 5 s, γ_s already consumed the remaining α , and the Mn concentration map remained virtually identical to the bimodal distribution of Mn in the initial condition as shown in Figure 4a. At 1000 s, the Mn concentration map indicates some Mn homogenization among the γ_p and γ_s .

Manganese concentration profiles across a selected γ - α interface in the initial simulation structure and after various times for the 750 and 850 $^{\circ}\text{C}$ SST simulations are plotted in Figure 6 for additional perspective on the Mn distribution results shown in Figures 4 and 5. Corresponding to the 750 $^{\circ}\text{C}$ SST simulation, Figure 6a indicates the change in the Mn distribution after a 1000 s secondary soak. The Mn gradient in the γ_p exhibits minimal change, while the γ_s is associated with an intermediate Mn concentration, and the remaining ferrite has been depleted in Mn. In Figure 6b, which corresponds to the 850 $^{\circ}\text{C}$ SST simulation, the Mn distribution associated with a 5 s secondary soak is nearly identical to the initial Mn distribution despite the γ_s having fully consumed the α . After a 1000 s secondary soak, some Mn redistribution is evident, but a high degree of heterogeneity remains; the central regions of γ_s and γ_p reflect the Mn

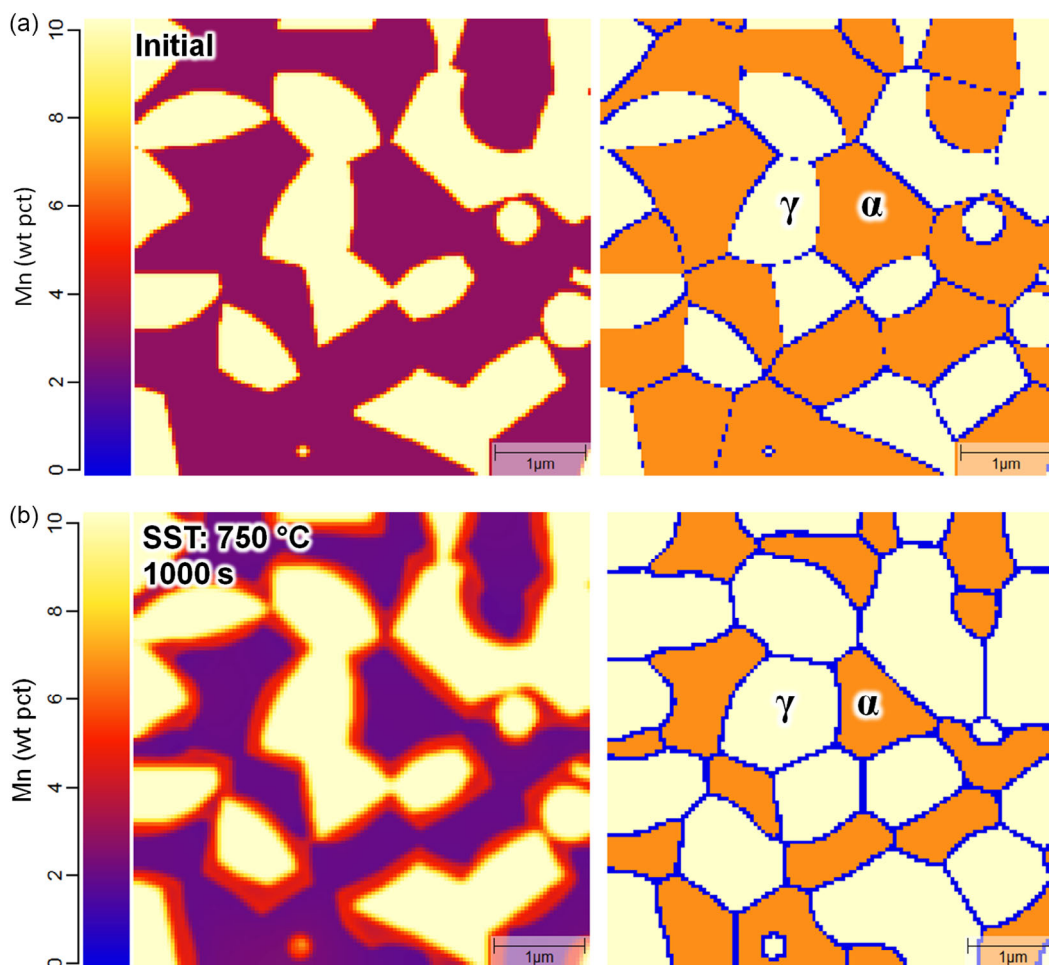


Figure 4. a) Initial structure for MICRESS simulations and b) results after a 1000 s secondary soak from a 750 °C secondary soaking temperature (SST) simulation. Mn distribution maps are shown on left and phase maps on right with regions of austenite (γ) and ferrite (α) labeled.

concentrations of α and γ , respectively, from the initial simulation structure.

4. Discussion

The interpreted microstructural evolution occurring during the DS treatments is summarized in **Figure 7** where the thermal profile with respect to time for the 660 °C PST sample is overlaid with schematics indicating the Mn partitioning and general phase-transformation behavior. Recrystallization and austenite formation occurred when the initial cold-rolled microstructure was heated and held at the PST. The growth of Mn-enriched γ_p occurred as Mn was transported through ferrite to the austenite–ferrite interface.^[20] As the γ_p continued to grow, the Mn distribution became increasingly bimodal as the ferrite was further depleted in Mn. Upon heating to the SST, growth of γ_s consumed the remaining ferrite and inherited the Mn-deficient concentration of the ferrite. This resulted in a fully austenitic microstructure during secondary soaking at 850 °C; however, the sluggish diffusion of Mn in austenite inhibited substantial Mn redistribution during the 5 s hold.

Thus, the Mn distribution remained relatively bimodal upon cooling from the SST. The Mn distribution in austenite caused a gradient in the austenite stability resulting in transformation of the Mn-deficient γ_s to martensite beginning at M_I , while transformation of the Mn-enriched γ_p initiated at M_{II} .

It should be noted that with a sufficient concentration of austenite-stabilizing solute, the γ_p may be fully retained to room temperature, in which case the M_{II} transformation would not be observed. While the DS concept is ideally intended to retain all of the γ_p , the present work was aimed at examining the ability to retain a variation in Mn concentration among a fully austenitic microstructure during the secondary soak step of DS. The nominal composition of the steel used in this study, having only a modest concentration of austenite-stabilizing additions for this family of steels, resulted in neither γ_p nor γ_s being fully retained upon final cooling. The absence of appreciable amounts of other austenite-stabilizing solute in the experimental alloy enabled the calculation of Mn concentrations associated with the γ_p and γ_s from the M_I and M_{II} temperatures.

Simulation results corresponding to the 850 °C SST (Figures 5 and 6b) support the suggested microstructural evolution as depicted in **Figure 7**. The γ_s formation is shown to inherit

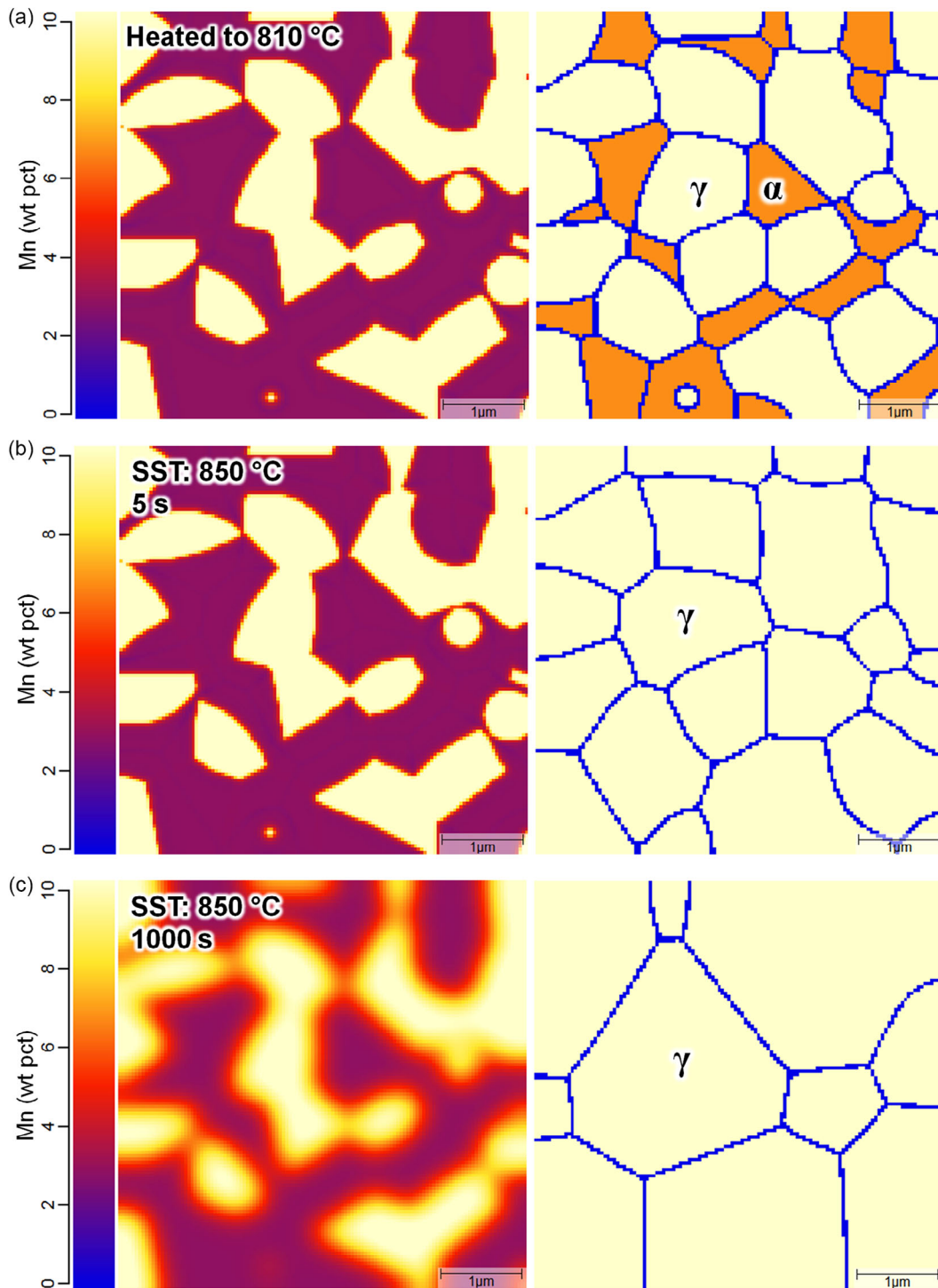


Figure 5. MICRESS results a) upon heating to 810 °C, b) after a 5 s secondary soak, and c) after a 1000 s secondary soak from the 850 °C SST simulation. Mn distribution maps are shown on left and phase maps on right with austenite (γ) and ferrite (α) regions labeled.

the Mn concentration of the α , resulting in a bimodal Mn concentration distribution among the γ_p and γ_s austenite. However, results from the 750 °C SST simulation suggest different transformation behavior during secondary soaking, resulting in γ_s with an intermediate Mn concentration which

did not fully consume the ferrite. The difference in these simulation predictions can be rationalized by considering the difference in diffusivity of Mn in ferrite and austenite, along with the local driving forces for austenite formation. With greater diffusivity in ferrite than in austenite, the growth of γ_s during

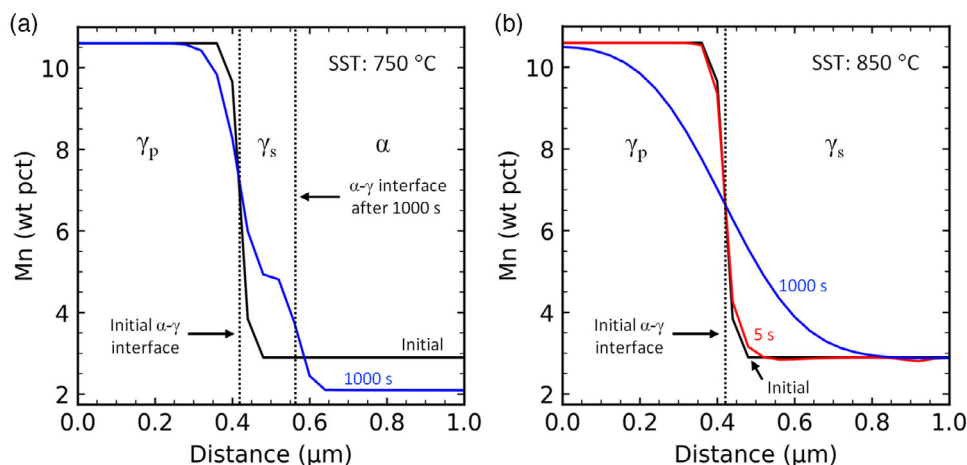


Figure 6. MICRESS predictions of Mn concentration profiles across austenite–ferrite interfaces in the initial simulation structure and at secondary soak times at SSTs of a) 750 °C and b) 850 °C. Regions labeled γ_p , γ_s , and α correspond to simulation results at 1000 s in a and at/after 5 s in b.

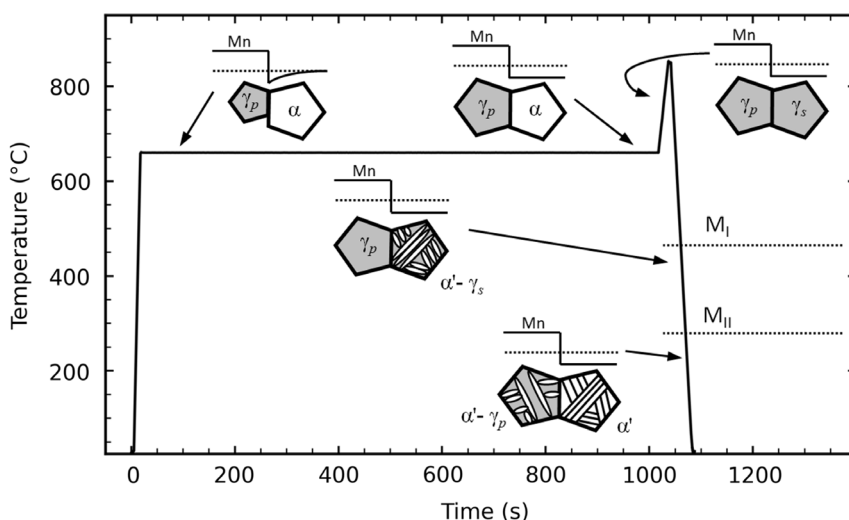


Figure 7. Thermal profile with respect to time for a sample that underwent a DS treatment with a PST of 660 °C. Schematics are overlaid summarizing the interpreted microstructure evolution and Mn distribution corresponding to various times during the DS treatment.

secondary soaking is dominated by Mn transport through ferrite to the γ_s – α interface rather than Mn redistribution in austenite; this condition is exacerbated as the γ_s – α interface advances into α and creates an additional buffer of γ_s between the γ_p and the γ_s – α interface. With γ_s formation predominantly influenced by the Mn concentration in the α , it is the Mn concentration in the remaining α which must be considered when predicting the relevant driving forces for γ_s formation and the associated phase-transformation mechanisms.

To consider the relevant driving forces for γ_s formation, Gibbs free energy–Mn concentration diagrams were constructed from Thermo-Calc calculations. The diagram for 750 °C is shown in **Figure 8a**. A red diagonal line was drawn to represent the common tangent between the austenite and ferrite curves. The red vertical lines are drawn at the tangents (approximately 2.2 and 4.8 wt% Mn) and indicate the boundaries between the α

single-phase, $\alpha + \gamma$ two-phase, and γ single-phase fields. The black, dashed vertical line drawn at 2.9 wt% Mn represents the Mn concentration in the ferrite after the primary soak at 640 °C; this is the equilibrium Mn concentration for ferrite and identical to the Mn concentration of ferrite in the initial simulation structure shown in **Figure 4a**. The diagram indicates that 2.9 wt% Mn is within the $\alpha + \gamma$ two-phase field at 750 °C. A magnified view of the boxed region in **Figure 8a** is shown in **Figure 8b**; a black, downward arrow indicates the driving force for transformation of α with a Mn concentration of 2.9 wt% to a two-phase mixture of α and γ with equilibrium Mn concentrations of approximately 2.2 and 4.8 wt%, respectively. Therefore, the growth of γ_s at 750 °C may be expected to proceed by means of a Mn-partitioning transformation where Mn diffuses through ferrite toward the γ_s – α interface as there is insufficient driving force for a partitionless, massive

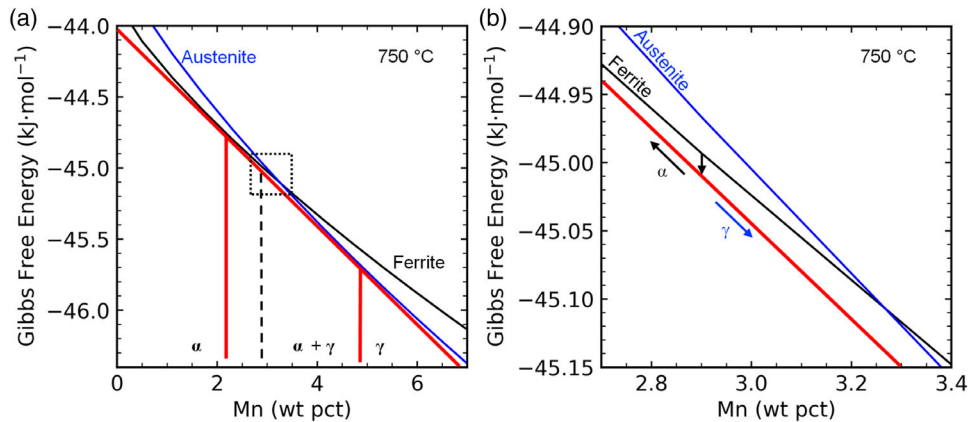


Figure 8. a) Gibbs free energy diagram for ferrite and austenite with respect to Mn concentration at 750 °C. Red, diagonal line indicates the common tangent of the austenite (blue curve) and ferrite (black curve). Solid, vertical lines intersect the common tangent line at the tangents in α and indicate the boundaries of the α , $\alpha + \gamma$, and γ phase fields. The dashed, vertical line indicates the equilibrium Mn concentration of ferrite at the PST of 640 °C (2.9 wt%). b) Enlarged view of boxed region in a. Black, downward facing arrow indicates the driving force for a partitioning transformation of ferrite with a Mn concentration of 2.9 wt% to an equilibrium mixture of ferrite and austenite with partitioned Mn. Black and blue, diagonal arrows labeled α and γ , respectively, indicate the corresponding partitioning behavior of the transformation products.

transformation. The simulation results shown in Figure 4b are consistent with this description and exhibit the eventual condition where the γ_s has formed with Mn enrichment relative to the ferrite, and the remaining ferrite has been further depleted in Mn.

Another Gibbs free energy–Mn concentration diagram is shown in Figure 9, which corresponds to 850 °C. In this diagram, 2.9 wt% Mn is within the γ single-phase field. The black, downward arrow indicates the driving force for a partitionless transformation of α with a Mn concentration of 2.9 wt% to γ with an identical Mn concentration. Therefore, the growth of secondary austenite at 850 °C may be expected to proceed by means of a

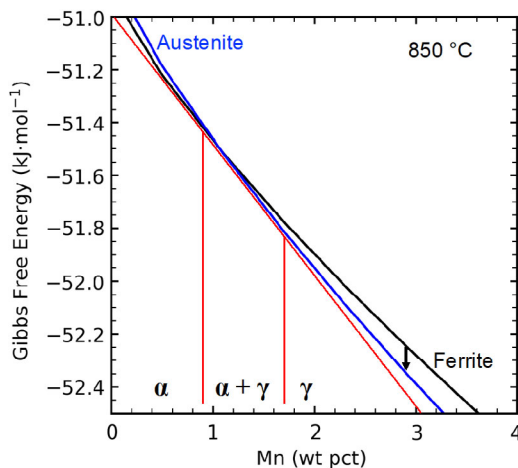


Figure 9. Gibbs free energy diagram for ferrite and austenite with respect to Mn concentration at 850 °C. Red, diagonal line indicates the common tangent of the austenite (blue curve) and ferrite (black curve). Vertical lines intersect the common tangent line at the tangents and indicate the boundaries of the α , $\alpha + \gamma$, and γ phase fields. Black, downward facing arrow indicates the driving force for a massive transformation of ferrite to austenite at 2.9 wt%.

massive transformation. The MICRESS results shown in Figure 5 are also consistent with a massive transformation of ferrite to austenite, which indicated that the γ_s had fully consumed ferrite and inherited the Mn concentration of ferrite during the transformation.

The differing simulation results in Figures 4 and 5 demonstrate that understanding the phase-transformation mechanism associated with γ_s formation is crucial to designing DS heat treatments with different desired Mn distributions. To produce a bimodal Mn distribution among a microstructure consisting entirely of austenite, the secondary soak temperature (and secondary heating rate) should be sufficient to avoid Mn-partitioning-induced growth of γ_s and, instead, induce a massive transformation causing the γ_s to readily consume the α and inherit the associated Mn concentration. The appropriate temperature to induce massive transformation is dependent on the chemical composition of the α formed during the primary soak. The simulation results shown in Figure 4b suggest that it may also be feasible to generate trimodal Mn distributions within a fully austenitic microstructure. This may potentially be accomplished by adding a third soak step to transform the remaining ferrite to austenite after the secondary soak at 750 °C. Furthermore, it is conceivable that a microstructure consisting of continuously Mn-graded austenite grains, from center to grain boundary, may be achieved through judicious control of the heating rate in a single-step austenitization treatment.

5. Conclusions

This work demonstrates the feasibility of developing and maintaining heterogeneous Mn distributions in austenite with the application of DS treatments. The phase-transformation mechanism associated with the formation of secondary austenite affects the Mn redistribution (or lack thereof) during secondary soaking. When the SST is sufficient to induce massive transformation of ferrite to austenite, a relatively rapid transformation of

the remaining ferrite to austenite occurs resulting in a bimodal Mn distribution among the fully austenitic microstructure that is virtually identical to the Mn distribution generated during primary soaking. If the SST is not sufficient to induce a massive transformation, relatively slow growth of secondary austenite with an intermediate Mn concentration proceeds at the expense of ferrite by a partitioning transformation where the Mn concentration in ferrite is further reduced as Mn is diffusively transported through ferrite to the advancing austenite interface. When a partitioning transformation during secondary soaking predominates, the composition of the secondary austenite is dependent on the secondary soaking temperature.

Acknowledgements

The authors gratefully acknowledge the support of Pacific Northwest National Laboratory, Los Alamos National Laboratory, the sponsors of the Advanced Steel Processing and Products Research Center at the Colorado School of Mines, and the ASM Material Genome Toolkit. This work was funded by the Department of Energy's Office of Vehicle Technologies under the Automotive Lightweighting Materials Program.

Conflict of Interest

The authors declare no conflict of interest.

Data Availability Statement

The data that support the findings of this study are available from the corresponding author upon reasonable request.

Keywords

massive transformations, medium-manganese steels, phase-field simulations, phase transformations, solute partitioning

Received: December 16, 2022

Revised: February 27, 2023

Published online:

-
- [1] R. L. Miller, *Metall. Mater. Trans. B* **1972**, 3 905.
[2] K. Steineder, D. Krizan, R. Schneider, C. Béal, C. Sommitsch, *Acta Mater.* **2017**, 139, 39.

- [3] R. S. Varanasi, M. Lipińska-Chwałek, J. Mayer, B. Gault, D. Ponge, *Scr. Mater.* **2022**, 206, 114228.
[4] J. Erno, P. Maugis, A. Perlade, *Comput. Mater. Sci.* **2016**, 125, 206.
[5] F. Huyan, J.-Y. Yan, L. Höglund, J. Ågren, A. Borgenstam, *Metall. Mater. Trans. A* **2018**, 49, 1053.
[6] J. T. Benzing, A. Kwiatkowski da Silva, L. Morsdorf, J. Bentley, D. Ponge, A. Dutta, J. Han, J. R. McBride, B. Van Leer, B. Gault, D. Raabe, J. E. Wittig, *Acta Mater.* **2019**, 166, 512.
[7] N. Nakada, K. Mizutani, T. Tsuchiyama, S. Takaki, *Acta Mater.* **2014**, 65, 251.
[8] J. Han, S.-J. Lee, J.-G. Jung, Y.-K. Lee, *Acta Mater.* **2014**, 78, 369.
[9] J. Han, Y.-K. Lee, *Acta Mater.* **2014**, 67, 354.
[10] E. De Moor, D. K. Matlock, J. G. Speer, M. J. Merwin, *Scr. Mater.* **2011**, 64, 185.
[11] P. J. Gibbs, E. De Moor, M. J. Merwin, B. Clausen, J. G. Speer, D. K. Matlock, *Metall. Mater. Trans. A* **2011**, 42, 3691.
[12] E. De Moor, J. G. Speer, D. K. Matlock, in *Proceedings of the First Int. Conf. on Automobile Steel and the 3rd Int. Conf. on High Manganese Steels* **2016**, p. 182–185.
[13] A. Glover, P. J. Gibbs, C. Liu, D. W. Brown, B. Clausen, J. G. Speer, E. De Moor, *Metals* **2019**, 9, 761.
[14] A. Glover, J. G. Speer, E. De Moor, *Front. Mater.* **2021**, 7, 622131.
[15] J. J. Mueller, X. Hu, X. Sun, Y. Ren, K. Choi, E. Barker, J. G. Speer, D. K. Matlock, E. De Moor, *Mater. Des.* **2021**, 203, 109598.
[16] M. Hillert, *Metall. Mater. Trans. A* **1984**, 15, 411.
[17] H. I. Aaronson, *Metall. Mater. Trans. A* **2002**, 33, 2285.
[18] T. B. Massalski, *Metall. Mater. Trans. A* **1984**, 15, 421.
[19] J. H. Perepezko, *Metall. Mater. Trans. A* **1984**, 15, 437.
[20] J. J. Mueller, D. K. Matlock, J. G. Speer, E. De Moor, *Steel Res. Int.* **2021**, 92, 2100298.
[21] J. J. Mueller, D. K. Matlock, J. G. Speer, E. De Moor, *Metals* **2019**, 9, 926.
[22] E. Gamsjäger, M. Wiessner, S. Schider, H. Chen, S. van der Zwaag, *Philos. Mag.* **2015**, 95, 2899.
[23] M. Hillert, *Met. Sci.* **1979**, 13, 118.
[24] G. P. Krielaart, S. van der Zwaag, *Mater. Sci. Technol.* **1998**, 14, 10.
[25] J. J. Wits, T. A. Kop, Y. van Leeuwen, J. Seitsma, S. van Der Zwaag, *Mater. Sci. Eng., A* **2000**, 283, 234.
[26] J. Kučera, K. Stránský, *Mater. Sci. Eng.* **1982**, 52, 1.
[27] B. De Cooman, J. G. Speer, *Fundamentals of Steel Product Physical Metallurgy*, Association for Iron and Steel Technology, Warrendale, PA, USA **2011**.
[28] P. Shewmon, *Diffusion in Solids*, The Minerals, Metals, and Materials Society, Warrendale, PA, USA **1989**.
[29] J. Mahieu, B. C. De Cooman, J. Maki, *Metall. Mater. Trans. A* **2002**, 33, 2573.